DOI: 10.1002/chem.200600127

An Experimental and Theoretical Investigation of Gas-Phase Reactions of Ca^{2+} with Glycine

Inés Corral,[a] Otilia Mó,[a] Manuel Yáñez,*[a] Jean-Yves Salpin,*[b] Jeanine Tortajada,[b] Damian Moran,[c] and Leo Radom*[c]

Abstract: The gas-phase reactions between Ca^{2+} and glycine ($[Ca(gly)]^{2+}$) have been investigated through the use of mass spectrometry techniques and B3-LYP/cc-pWCVTZ density functional theory computations. The major peaks observed in the electrospray MS/MS spectrum of $[Ca(gly)]^{2+}$ correspond to the formation of the $[Ca,C,O_2,H]^+$, $NH_2CH_2^+$, $CaOH^+$, and $NH_2CH_2CO^+$ fragment ions, which are produced in Coulomb explosion processes. The computed potential energy surface (PES) shows that not only are these species the most stable product ions from a thermodynamic point of view, but they may be produced with barriers lower than for competing processes. Carbon monoxide is a secondary product, derived from the unimolecular decomposition of some of the primary ions formed in the Coulomb explosions. In contrast to what is found for the reactions of Ca^{2+} with urea ($[Ca(urea)]^{2+}$), minimal unimolecular losses of neutral fragments are observed for the gas-phase fragmentation processes of $[Ca(gly)]^{2+}$, which is readily explained in terms of the topological differences between their respective PESs.

Keywords: ab initio calculations · amino acids · calcium · Coulomb explosion · gas-phase reactions · mass spectrometry

Introduction

The study of gas-phase ion–molecule reactivity is quite often crucial to the understanding of the behavior of many biochemical systems and many biological processes, because these take place in essentially nonpolar environments and cannot always be rationalized in terms of reactivity in solution. A paradigmatic example is provided by uracil. It has been well established that the pK_a values in water for the N1 and N3 sites of uracil are virtually the same,[1] whereas the corresponding gas-phase acidities differ by more than 40 kJ mol^{-1}. Interestingly, the stability of anionic uracil in the active site of uracil–DNA glycosylase, established by means of contemporary NMR techniques,[2] is consistent with the enhanced intrinsic acidity of the N1 site, and contrary to the expectation based on solution acidities.[3] Similarly, gas-phase studies of the interaction of metal cations with amino acids can provide useful insights into the corresponding interactions with more complex biologically relevant systems such as peptides or proteins. In this respect, glycine represents the simplest model for such a theoretical and experimental investigation.

To date, most efforts to determine the intrinsic reactivity of cationized small model biomolecules[4–8] have concentrated on singly charged ions, in spite of the biochemical importance of interactions with multiply charged ions. This is exemplified by the combined theoretical and experimental studies on reactions of glycine with Ni^+ and Cu^+, which showed that the most important reactive pathways are those leading to the loss of H_2O, CO and $[C,H_2,O_2]$.[9,10] Studies of the analogous reactions involving metal dications are important because of the role they play in the structural stability of biopolymers, as well as in many of the biological func-

[a] Dr. I. Corral, Prof. O. Mó, Prof. M. Yáñez
Departamento de Química, C-9
Universidad Autónoma de Madrid
Cantoblanco, 28049-Madrid (Spain)
E-mail: manuel.yanez@uam.es

[b] Dr. J.-Y. Salpin, Prof. J. Tortajada
Laboratoire d'Analyse et de Modélisation pour la Biologie et l'Environnement, UMR
CNRS 8587, Université d'Evry Val d'Essonne
Bâtiment Maupertuis, Boulevard François Mitterrand, 91025 Evry Cedex (France)
E-mail: jean-yves.salpin@univ-evry.fr

[c] Dr. D. Moran, Prof. L. Radom
School of Chemistry, University of Sydney
Sydney, NSW 2006 (Australia)
E-mail: radom@chem.usyd.edu.au

Supporting information for this article is available on the WWW under http://www.chemeurj.org/ or from the author.

tions of proteins and nucleic acids. For example, alkaline-earth and transition-metal dications participate in the maintenance of the structure of folded proteins, nucleic acids, and biological membranes, and are common cofactors in metalloproteins. In particular, Ca^{2+} takes part in a wide range of biological processes, including the regulation of muscle contraction, transduction, glycolysis, gluconeogenesis, ion transport and the stabilization of interprotein complexes.[11,12]

Dissociative electron ionization (DEI) and photoionization (PI) are longstanding techniques that have been used for the determination of thermochemical information for gas-phase multiply-charged cations.[13–15] More recently, the advent of electrospray ionization (ESI) has provided an attractive method for generating gas-phase multiply charged clusters from aqueous solution.[16] However, studies on the gas-phase reactions of dicationic complexes $[M{\cdot}B]^{2+}$ are still not common, because of difficulties in generating thermodynamically or kinetically stable dications in the gas phase.[17,18] The bonds in B within the $[M{\cdot}B]^{2+}$ complex are activated and, under typical mass spectrometry conditions, it is normal to observe spontaneous loss of a proton from the base B. This limits the accessibility of the doubly charged $[M{\cdot}B]^{2+}$ complex, and the unimolecular reactivity of the deprotonated $[M{\cdot}(B{-}H)]^{+}$ species is more readily observed. Although this is generally the case when dealing with transition-metal dications, we recently found for complexes of Ca^{2+} with urea that deprotonation is endothermic and that the $[Ca{\cdot}urea]^{2+}$ dication could be isolated and its subsequent reactivity analyzed.[19] This analysis was facilitated by knowledge of the $[Ca{\cdot}urea]^{2+}$ potential energy surface (PES), which was achieved through quantum-chemistry computations.

Our previous study of the reactions between Ca^{2+} and urea[19] was carried out with the ultimate goal of modeling the reactivity of Ca^{2+} with nucleic acids, peptides, and proteins. In that study, the mass spectrum of $[Ca(urea)]^{2+}$ showed spontaneous losses of neutral HNCO and NH_3, in addition to peaks corresponding to the NH_2CO^+, $CaNH_2^+$, and $[Ca,N,C,O]^+$ monocations that are produced in Coulomb explosion processes. To help in the understanding of the experimental results, we also carried out computations using the B3-LYP functional together with the cc-pWCVTZ basis set. We had previously found this combination to provide a good compromise between accuracy and computational cost when calculating Ca^{2+} binding energies.[20] This is therefore the theoretical approach chosen for the computations in the present paper, in which we use experiment and theory to examine how the reactivity pattern of the complex of Ca^{2+} with the first member in the series of natural amino acids, namely glycine, compares with that of $[Ca(urea)]^{2+}$.

Methods

Experimental details: Electrospray mass spectra were recorded on a QSTAR PULSAR i (Applied Biosystems/MDS Sciex) hybrid instrument (QqTOF) fitted with a nanospray source to minimize transfer-line contamination. Several μL of aqueous mixtures of calcium chloride (10^{-4} mol L^{-1}) and glycine (10^{-4} mol L^{-1}) were nanosprayed (20–50 nL min^{-1}) using borosilicate emitters (Proxeon). Samples were ionized by using an 800–900 V nanospray needle voltage and the lowest possible nebulizing gas pressure (tens of millibars). The declustering potential (DP, also known as "cone voltage"), defined as the difference in potentials between the orifice plate and the skimmer (grounded), ranged from 0 to 30 V. To improve ion transmission and subsequently sensitivity during the experiments, collision gas (CAD, N_2) was present at all times for collisional focusing in both the Q0 (ion guide preceding Q1 and located just after the skimmer) and Q2 (collision cell) sectors. For MS/MS spectra, ions of interest were mass-selected by using quadrupole Q1, and allowed to collide with nitrogen gas at various collision energies ranging from 6.5 eV to 16 eV in the laboratory frame (the collision energy is given by the difference between the potentials of Q0 and Q2), with the resulting fragments separated by the time-of-flight (TOF) analyzer after orthogonal injection. Low gas pressures (typically 10^{-5} mbar) were used to limit multiple ion–molecule collisions. Glycine (both labeled and unlabeled) and calcium chloride were purchased from Aldrich and used without further purification. All experiments were performed in Milli-Q purified water.

Computational details: Geometries were optimized by using density functional theory with the hybrid functional B3-LYP,[21,22] as implemented in the Gaussian 03 suite of programs,[23] in conjunction with the correlation-consistent polarized core-valence triple-zeta cc-pWCVTZ basis set.[24] The cc-pWCVTZ basis includes core-correlation functions, which are important for the accurate treatment of alkaline-earth metal oxides and hydroxides.[25,26] Note that basis set superposition error (BSSE) has not been considered in the present study, as the B3-LYP/cc-pWCVTZ combination usually has very small BSSE corrections.[20] Harmonic vibrational frequencies were computed (at the same level) to classify stationary points as local minima or transition structures (TS), and to estimate their zero-point vibrational energy (ZPVE) corrections (scaled by 0.985[24]). Intrinsic reaction coordinate (IRC) computations were used to confirm the connection between the transition structures and their adjacent minima.

Further insight into the nature of $[Ca(gly)]^{2+}$ bonding was gained by using the atoms-in-molecules approach.[27] For this purpose, we located bond critical points and calculated the charge density values associated with them so as to be able to compare bond strengths. To assess the nature of the interactions, contour maps were obtained of the energy density ($H(\mathbf{r})$), defined in Equation (1),

$$H(\vec{r}) = \frac{1}{4}\nabla^2\rho(\vec{r}) - G(\vec{r}) \qquad (1)$$

where $\nabla^2\rho(\vec{r})$ and $G(\vec{r})$ are the laplacian of the electron density and the kinetic energy density, respectively. Covalent

bonds, in which the potential term dominates over the kinetic term, are characterized by negative values of the energy density. Conversely, ionic linkages, where the kinetic term dominates, are characterized by positive values of H(**r**).

Results and Discussion

Mass spectrometry experiments: A typical nano-electrospray spectrum obtained at DP = 10 V for a 1:1 aqueous mixture of $CaCl_2$/glycine is displayed in Figure 1. As previously observed during our $[Ca(urea)]^{2+}$ study,[20] several ion types are detected. Hydrated Ca^{2+} dications ($[Ca(H_2O)_m]^{2+}$; m = 1–4) appear at *m/z* 28.99, 37.99, 46.99, and 55.99, respectively. The $[Ca(H_2O)_m]^{2+}$ peaks are generally less intense than that for calcium hydroxide monocation ($CaOH^+$; *m/z* 56.96) for all the DP values employed, and progressively disappear as the DP increases. $[Ca(gly)_n]^{2+}$ complexes (n = 1, 2) are detected in significant abundance at *m/z* 57.49 and 95.01, while a third dication species at *m/z* 66.5 is attributed to $[Ca(gly).H_2O]^{2+}$. The 2+ charge in these complexes is readily confirmed by making comparisons with the 1-^{13}C-glycine spectrum (see Figure 1 insert), as their mass-to-charge ratio is shifted by 0.5, 1, and 0.5 Thomson, respectively. Note that observation of the $[Ca(gly)_n]^{2+}$ and $[Ca(gly)\cdot H_2O]^{2+}$ complexes is not straightforward and requires soft (low DP) energetic source/interface conditions. The intensity of the $[Ca(gly)]^{2+}$ peak is a maximum at 0 V DP, while increasing the DP results in fragmentation and formation of a deprotonated $[Ca(gly)-H]^+$ complex at *m/z* 113.98. It is worth mentioning that the resolving power of the TOF is particularly helpful when distinguishing the $[Ca(gly)]^{2+}$ dication (*m/z* 57.49) from calcium hydroxide monocation (*m/z* 56.96), a distinction that could not be achieved with a triple–quadrupole instrument alone. The protonated form of glycine is detected at *m/z* 76.03, although this could in principle also correspond to $[Ca(H_2O)_2]^+$ generated by dissociative charge-transfer from $[Ca(H_2O)_3]^{2+}$. However, according to a recent DFT study,[28] this dissociative charge transfer process is unfavorable, regardless of the alkaline-earth metal considered (Be, Mg, Ca, Sr, or Ba). This is confirmed in the present work both by the accurate mass measurement and the MS/MS spectrum, which exhibits an abundant loss of carbon monoxide and formation of the $CH_2{=}NH_2^+$ ion at *m/z* 30.

To examine the unimolecular reactivity of the $[Ca(gly)]^{2+}$ complex, we have carried out a series of MS/MS experiments. The first analyser (Q1) of our QqTOF is unable to properly distinguish the $[Ca(gly)]^{2+}$ complex (*m/z* 57.49) from the $CaOH^+$ cation (*m/z* 56.96). Consequently, we used labeled glycine to shift the *m/z* ratio of the former and ensure correct parent ion selection. The MS/MS spectra obtained with 1-^{13}C-glycine and 2,2-[D_2]-glycine are shown in Figure 2. The unimolecular reactivity appears to be different from that observed for the $[Ca(urea)]^{2+}$ system,[20] as there is almost no loss of neutral molecules. The elimination of ammonia, leading to the peak at *m/z* 50, is observed in Figure 2b, but only to a relatively minor extent. Examination of Figure 2a shows that four characteristic fragment ions are observed, at *m/z* 30, 57, 59, and 86. The *m/z* 30 species certainly corresponds to the $NH_2{=}CH_2^+$ ion, as its mass-to-charge ratio is shifted by 2 Thomsons when using 2,2-[D_2]-glycine. The methylenimmonium cation, together with the *m/z* 86.0 species (85.0 in Figure 2b), which includes the C(1) atom and corresponds to $[Ca,C,O_2,H]^+$, may be generated through a Coulomb explosion process. The most abundant fragment in the case of the 1-^{13}C-glycine complex corresponds to $CaOH^+$ (*m/z* 57), which is also produced by a Coulomb explosion that additionally yields an *m/z* 59 species (Figure 2a). When 1-^{13}C-glycine is replaced by 2,2-[D_2]-glycine, the *m/z* 57 peak remains, while the *m/z* 59 peak (Figure 2a) is shifted by 1 Thomson to *m/z* 60 (Figure 2b), which is consistent with ^{13}C removal and addition of two deuterium atoms. Therefore, Figure 2a and 2b allow us to conclude that the ions at *m/z* 59 and 60 contain both C(1) and C(2) centers, and could correspond to a $[C_2,H_4,N,O]^+$ species that is generated together with the $[CaOH]^+$ monocation.

One might have expected the partner peaks arising from a Coulomb explosion to be of equal intensity, but this is not

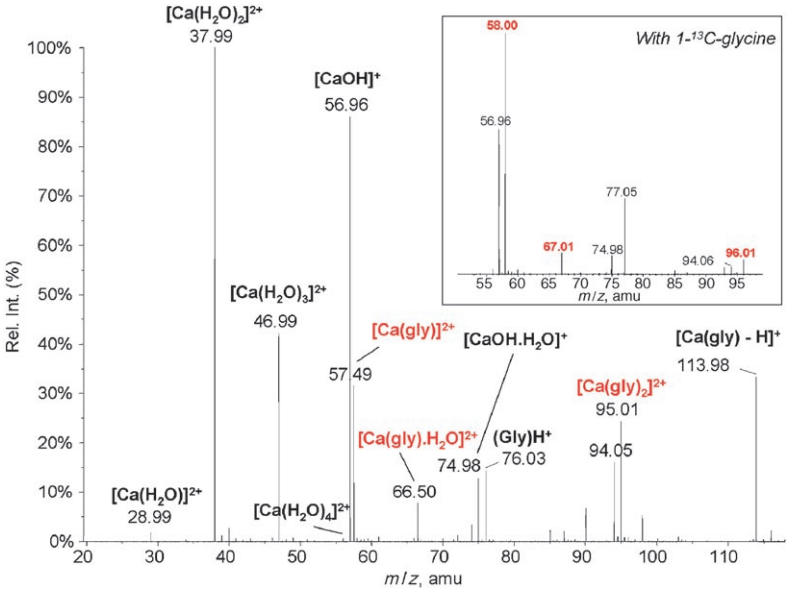

Figure 1. Positive nano-electrospray spectrum of an aqueous $CaCl_2$/glycine (10^{-4} mol L^{-1}/10^{-4} mol L^{-1}) mixture, recorded with a declustering potential of 10 V.

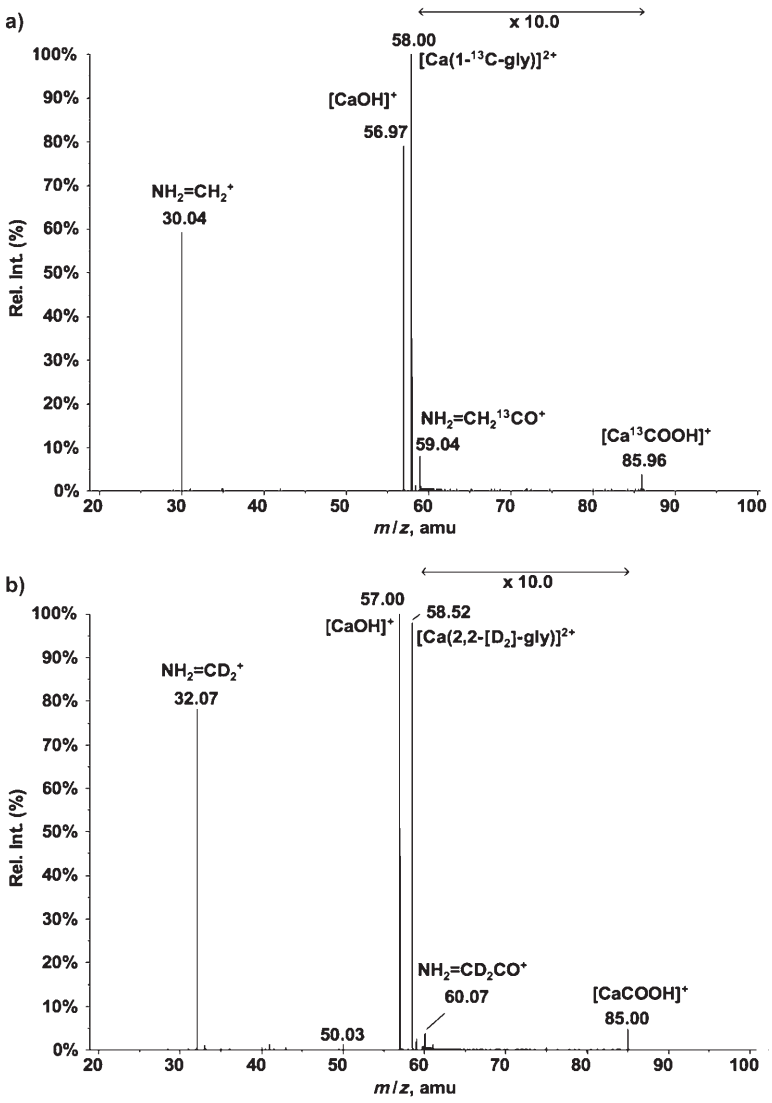

Figure 2. Low-energy CID spectra of the $[Ca(gly)]^{2+}$ complex obtained with a) 1-^{13}C-glycine and b) 2,2-$[D_2]$-glycine recorded with a collision energy of 11 eV (laboratory frame).

the case in our MS/MS spectra. Instead, the *m/z* 30 and *m/z* 57 peaks (Figure 2a) are significantly more intense than their counterpart peaks at *m/z* 86 and *m/z* 59, respectively. This is the reverse of our previous observations for $[Ca(urea)]^{2+}$,[20] where the Coulomb explosion leading to ions with *m/z* 18 and 82 produced a lower abundance of the lighter ion. This phenomenon was interpreted in terms of different radial ion energies, with the lighter ions generated by the Coulomb explosion gaining most of the radial energy and therefore having a much higher velocity than the relatively high mass ions. This can result in an unstable ion trajectory within the instrument and explains why lighter ions are usually not detected in the MS/MS spectrum. In the present case, this phenomenon cannot account for the large intensity difference between *m/z* 57 and 59 ions, which have similar masses. A more plausible explanation is that the *m/z* 59 and 86 ions (*m/z* 60 and 85 for 2,2-$[D_2]$-glycine) may undergo secondary fragmentation (loss of ^{13}CO) leading to ions with *m/z* 30 and 57, respectively (Figure 2a). This is possible if one assumes that *m/z* 59 and 86 ions correspond to $NH_2CH_2{}^{13}CO^+$ and $[Ca,{}^{13}C,O_2,H]^+$, respectively. We therefore propose the fragmentation shown in Scheme 1, where the *m/z* values given in italics correspond to those observed for the 2,2-d_2-glycine. In addition to a decrease in the intensity of the *m/z* 59 and 86 peaks, the fragmentation pattern in Scheme 1 will result in a concomitant increase in the *m/z* 30 and 57 peak intensities.

The mechanism outlined in Scheme 1 is consistent with the changes in the spectra that are observed as the collision energy is increased from 8 eV (laboratory frame) to 16 eV. These show in the case of $[Ca(2,2\text{-}[D_2]\text{-glycine})]^{2+}$ (see Figures S1–S5 in the Supporting Information) that the peaks at *m/z* 32 and 57 become increasingly dominant, while those for the corresponding parent ions at *m/z* 60 and 85 practically disappear by the time a 16 eV collision energy is reached. The dominance of the *m/z* 32 and 57 peaks as the collision energy is increased is also shown in Figure S6. As we shall also show below, these

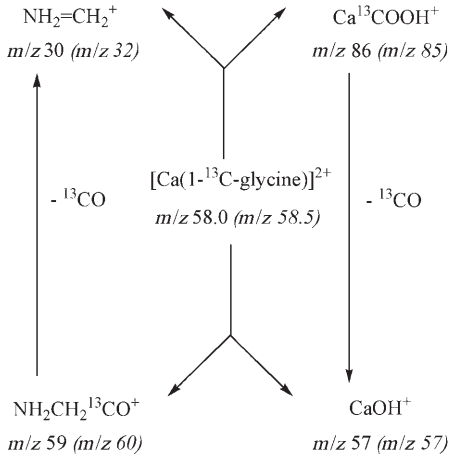

Scheme 1. Proposed fragmentation Scheme for $[Ca(1\text{-}^{13}C\text{-glycine})]^{2+}$ and $[Ca(2,2\text{-}[D_2]\text{-glycine})]^{2+}$ (*m/z* values in parentheses correspond to $[Ca(2,2\text{-}[D_2]\text{-glycine})]^{2+}$).

findings are consistent with our theoretical finding that the reactions corresponding to loss of CO from the *m/z* 59 and 86 ions have low-energy requirements.

To better rationalize these experimental findings and to test our assumptions, we have used theoretical calculations to explore the $[Ca(gly)]^{2+}$ potential energy surface and describe the bonding characteristics of the most stable complexes.

Structures and stabilities of $[Ca(gly)]^{2+}$: We have considered the coordination of Ca^{2+} to the various basic sites of neutral glycine, as well as to the glycine zwitterion. The optimized $[Ca(gly)]^{2+}$ geometries and their relative energies are summarized in Figure 3. Attachment of Ca^{2+} to the two oxygen atoms of zwitterionic glycine leads to the most stable isomer (**1**), in agreement with previous theoretical calculations carried out at the MP2 level,[29] and at the B3-LYP and MP2

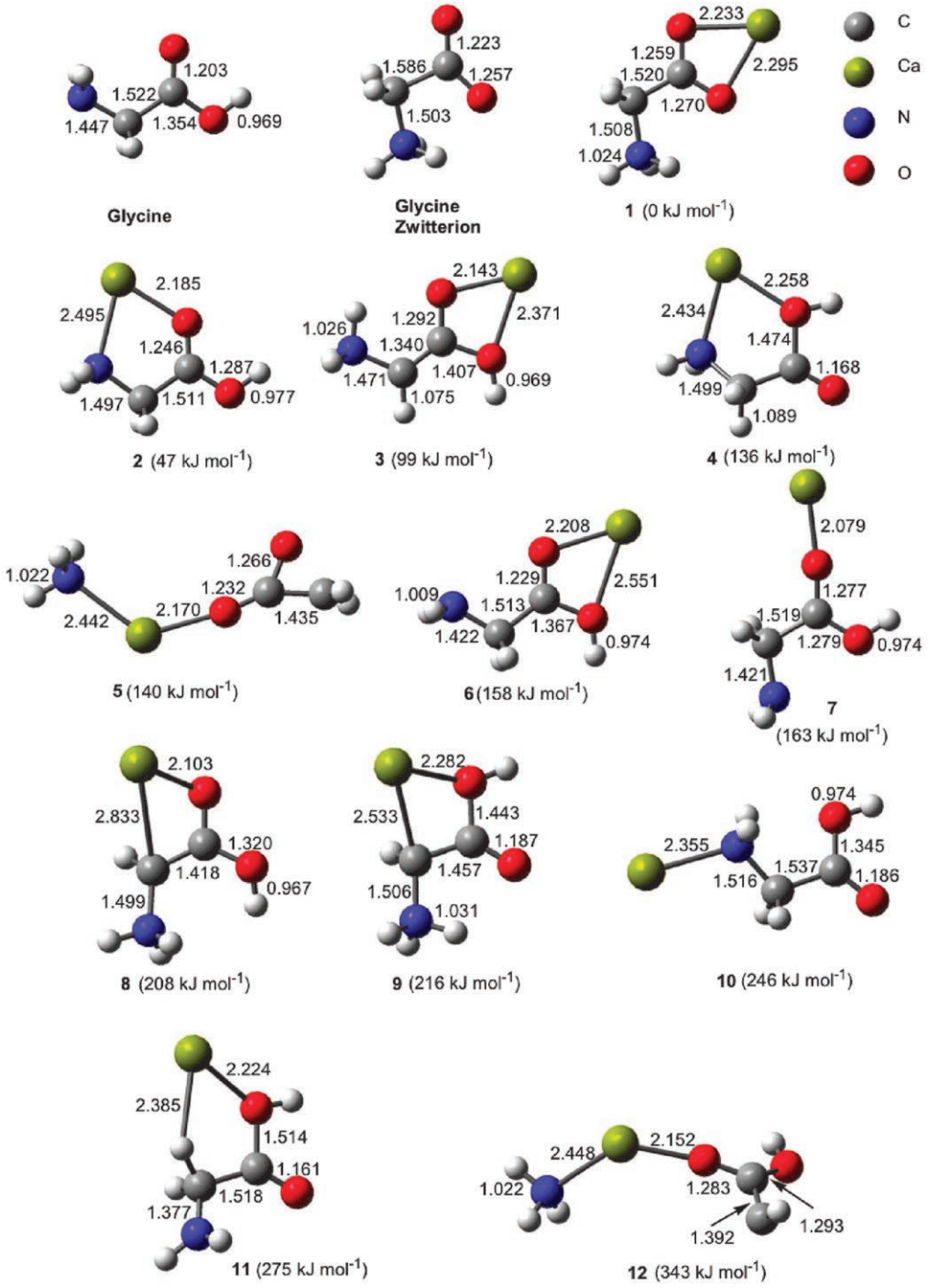

Figure 3. Optimized B3-LYP/cc-pWCVTZ geometries (Å) for glycine and isomeric $[Ca(gly)]^{2+}$ structures. Relative energies ($kJ\,mol^{-1}$) are given in parentheses. For the zwitterionic form of glycine, the structure shown was obtained by constraining the N–H bond lengths to be the same as those in complex **1**, in order to avoid collapse to the neutral isomer.

levels using effective-core potentials.[30] More generally, the lowest energy structures (**1**–**4**) correspond to bridged complexes, in which the metal dication interacts with multiple glycine centers. Complexes **2** and **4** form five-membered-ring structures, with the Ca^{2+} dication simultaneously coordinated to an oxygen and a nitrogen atom, while in **3** the Ca^{2+} is bonded to the two oxygen atoms of an ylide-type form of glycine. Analogues of complex **2** have previously been found to be the most stable species on the PESs for complexes of glycine with Li^+, Na^+, Cu^+, and Ni^+.[9,31–33] We have also located structures **7** and **10**, where glycine acts as a monodentate base. In these complexes, which are relatively high in energy (Figure 3), Ca^{2+} interacts exclusively with either the carbonyl or the amino group. Also high in energy lie complexes **8** (208 kJ mol^{-1}) and **9** (216 kJ mol^{-1}), in which Ca^{2+} interacts with the methine carbon atom and with the carbonyl or hydroxyl oxygen, respectively, of an ylide-type structure of glycine. The remaining minima that we have located on the PES, namely structures **5** and **12**, correspond to bisligated complexes of Ca^{2+} with NH_3 and $[C_2,H_2,O_2]$ moieties.

Bonding in $[Ca(gly)]^{2+}$: The bonding between Ca^{2+} and glycine in the $[Ca(gly)]^{2+}$ complexes is essentially ionic. This is demonstrated by the energy density contour maps of isomers **1** and **2** (Figure 4), which have positive H(**r**) values in the region between Ca^{2+} and the base. This finding is also supported by the small values of the charge density at the Ca–O and Ca–N bond critical points (see Figure 5), as is typical of conventional ionic linkages. As a result of the strong ionic bonding in the $[Ca(gly)]^{2+}$ complexes, polarization effects are very important, as the Ca^{2+} causes a significant reorganization of the glycine charge density and results in the activation of several bonds. For example, on going from neutral glycine to complex **2** (Figure 5), the charge density at the C=O and C–N bond critical points significantly decreases, by 0.043 and 0.031 e au^{-3}, respectively. Accordingly, the C=O and C–N distances lengthen by 0.043 and 0.049 Å, while the C–C and C–OH bonds shorten by 0.011 and 0.067 Å, respectively. Their stretching frequencies are concomitantly red-shifted by 151 (C=O) and 110 (C–N) cm^{-1}. For the zwitterionic form of glycine, Ca^{2+} attachment leads to reductions of 0.030 and 0.010 e au^{-3} in the charge density at the two C=O bond critical points, and to a concomitant lengthening of 0.036 and 0.013 Å, while the C–C distance shortens by 0.066 Å.

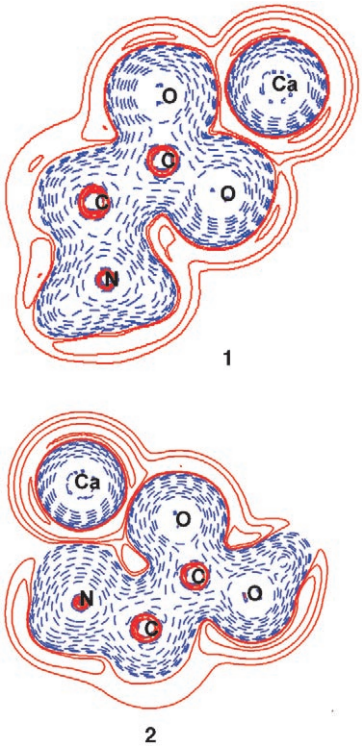

Figure 4. Contour maps of the energy density for $[Ca(gly)]^{2+}$ complexes **1** and **2**. Blue dashed lines and solid red lines correspond to negative and positive values of H(**r**), respectively.

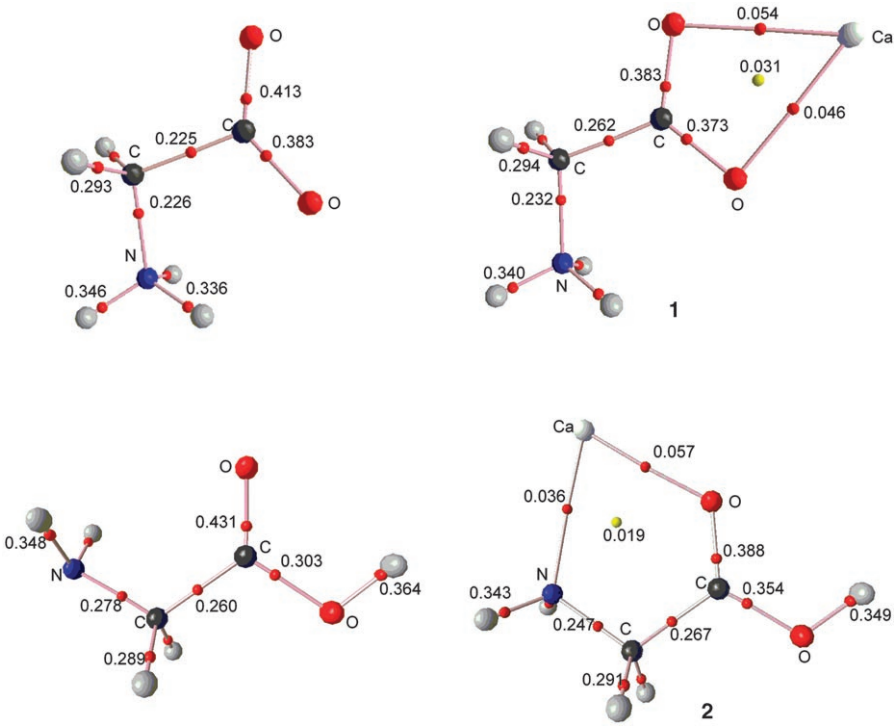

Figure 5. Molecular graphs of glycine, in its zwitterionic and neutral forms, and complexes **1** and **2**, showing the bond critical points (bcps; red) and the ring critical points (yellow). Electron densities are in e au^{-3}.

Rearrangement and fragmentation pathways of $[Ca(gly)]^{2+}$: ***1) Reactions originating from 1:*** Figure 6 shows the PES associated with rearrangement and fragmentation pathways originating from the global minimum energy structure **1**, which corresponds to complexation of Ca^{2+} with the zwitterionic form of glycine. The zwitterionic form of glycine is the dominant form in solution and, due to the softness of the ESI technique employed to form dications, one should expect the complex between Ca^{2+} and glycine zwitterion present in solution to persist in the gas phase, where in addition our calculations predict that it represents the most stable structure. Hence, we shall initially focus our attention on the unimolecular reactivity of form **1**. As illustrated in Figure 6, three Coulomb explosions have their origin in this complex. The most favorable one (with a barrier of 233 kJ mol^{-1}) leads to the dissociation of **1** (via **TS1b**) into $CaOH^+$ (*m/z* 57) and $NH_2CH_2CO^+$ (*m/z* 58),[34] which are two of the products detected experimentally in the MS/MS spectra (e.g., *m/z* 57 and *m/z* 60 in the spectrum involving the 2,2-$[D_2]$ isotopomer of glycine in Figure 2b). The other two Coulomb explosions leading (via **TS1a**) to NH_4^+ (*m/z* 18) + $CHCO_2Ca^+$ (*m/z* 97) or (via **TS1c**) to CO_2Ca^+ (*m/z* 84) + $NH_3CH_2^+$ (*m/z* 31) involve much higher (308 and 316 kJ mol^{-1}, respectively) barriers.

The zwitterionic complex **1** can also rearrange, in a low-energy process via **TS6–1** at 164 kJ mol^{-1}, to the transient intermediate **6**. From this point, Coulomb explosion via **TS6a** at 202 kJ mol^{-1} would yield the most stable fragments in Figure 6, namely $COCaOH^+$ (*m/z* 85) and $NH_2CH_2^+$ (*m/z* 30), at −66 kJ mol^{-1}. These correspond, for example, to the *m/z* 85 and *m/z* 32 peaks in the MS/MS spectrum involving the 2,2-$[D_2]$ isotopomer of glycine in Figure 2b. Alternatively, Coulomb explosion via **TS6b** at 231 kJ mol^{-1} would produce $CaOH^+$ (*m/z* 57) + $NH_2CH_2CO^+$ (*m/z* 58), as obtained also directly from **1**. As an aside, we note that it is possible that in the vicinity of **TS6–1**, a small part of the flux is directed to the loss of NH_3 at 356 kJ mol^{-1}, which might account for the weak *m/z* 50 peak found in the 2,2-$[D_2]$-glycine MS/MS spectrum (Figure 2b).

In summary, Coulomb explosion processes originating from the zwitterionic complex **1**, either in direct reactions or via the intermediate **6**, can account for all of the products detected in the experimental MS/MS spectra.

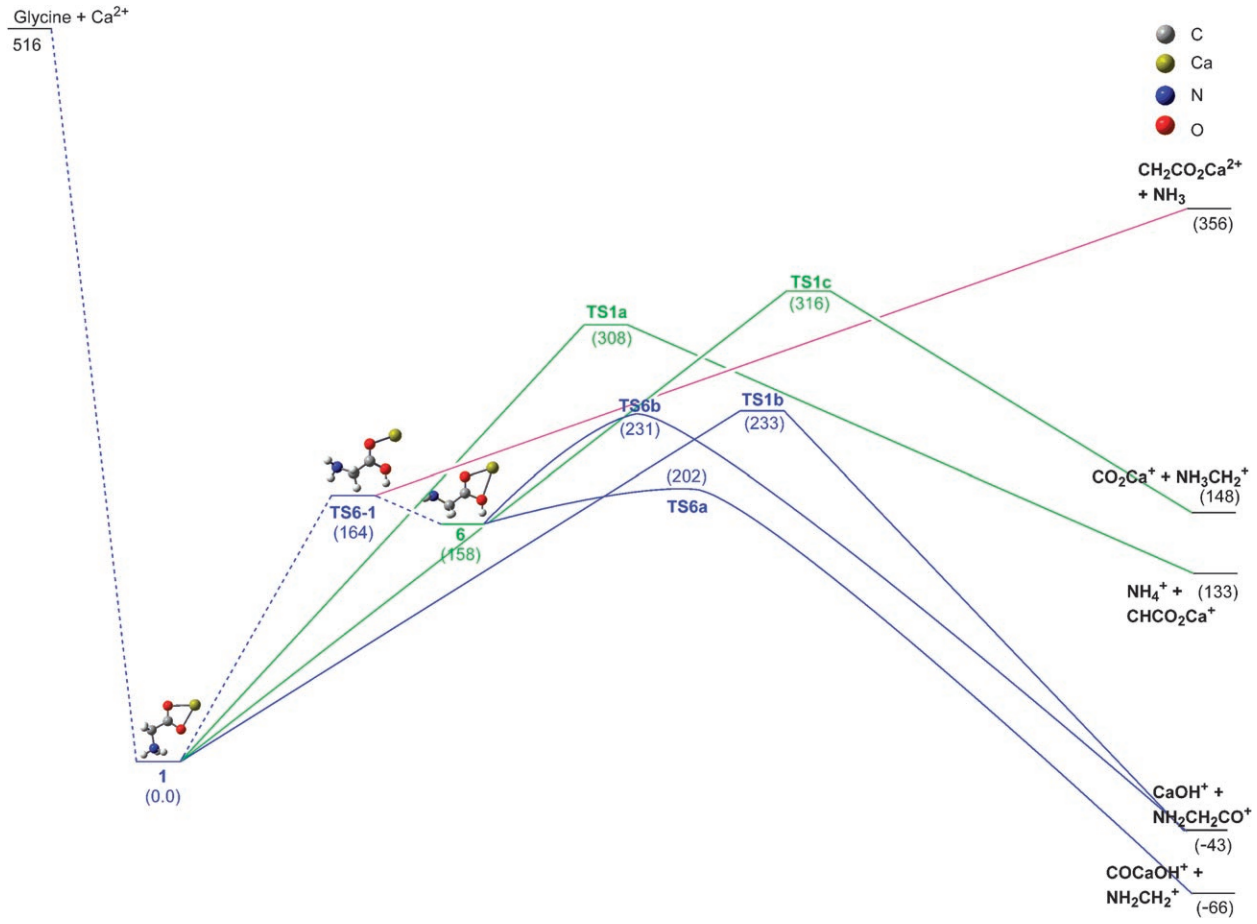

Figure 6. Schematic energy profile corresponding to the unimolecular reactivity for complexes of Ca^{2+} with zwitterionic glycine (**1**). The mechanisms originating from **1** that lead to the most favorable Coulomb explosions are shown in blue. Slightly higher energy processes originating from **1** are shown in green. The pink lines indicate the mechanisms associated with the still higher energy loss of NH_3. Relative energies (kJ mol^{-1}) are given in parentheses.

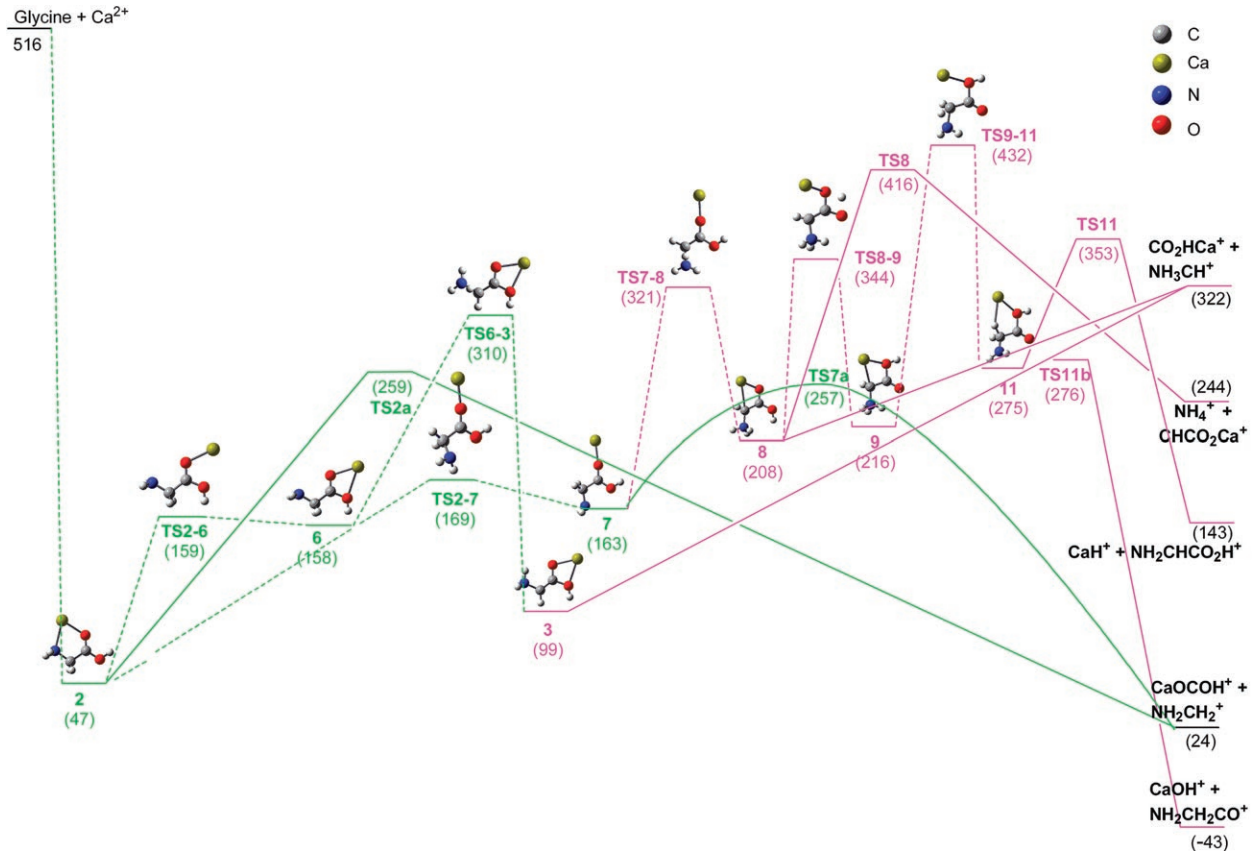

Figure 7. Schematic energy profile corresponding to the unimolecular reactivity for complexes of Ca^{2+} with neutral glycine (**2**). Medium energy processes originating from **2** are shown in green. Pink lines indicate the mechanisms associated with the still higher energy Coulomb explosions. Relative energies ($kJ\,mol^{-1}$) are given in parentheses.

2) Reactions originating from 2: Figure 7 shows rearrangement and fragmentation pathways originating from the most stable adduct of Ca^{2+} with neutral glycine, that is, **2**. This isomer can be produced from **1** via **6**, or by direct attachment of Ca^{2+} to the neutral form of glycine. Complex **2** can explode, via **TS2a** at 259 $kJ\,mol^{-1}$, to yield $CaOCOH^+$ (*m/z* 85) plus $NH_2CH_2^+$ (*m/z* 30). The same product ions can also be formed from adduct **2** via the intermediate **7** and **TS7a** at 257 $kJ\,mol^{-1}$. We note that these ions, which have an energy of 24 $kJ\,mol^{-1}$ relative to **1**, have the same mass as the ions $COCaOH^+$ plus $NH_2CH_2^+$ produced from **1** but they represent a higher energy combination and require higher energy TSs. If both the lower-energy pathway from **1** and the higher-energy pathway from **2** are in fact followed, this would mean that the $[Ca,C,O_2,H]^+$ (*m/z* 85) ions observed in the MS/MS spectra would correspond to a mixture of two different type of species, that is, those (produced from **1**) in which the calcium is inserted between the carbonyl and the hydroxyl moieties and those (produced from **2**) in which Ca^{2+} bridges the carbon and the oxygen atoms of the carbonyl group (see Figure 8).

Other reaction pathways starting from **1** or **2** and involving the intermediates **3**, **6**, or **7** are possible (Figure 7) but, since all of them are high-energy processes, they are discussed in the Supporting Information. The same applies to the mechanisms involving bisligated $[NH_3{-}Ca{-}C_2H_2O_2]^{2+}$ and other Ca–N bonded isomers, where the PES is presented in Figure S7 and discussed in the Supporting Information.

3) Summary remarks concerning the potential energy surface: The high energies predicted by the B3-LYP/cc-pWCVTZ computations for the fragmentation products and transition structures associated with species **3**, **8**, **9**, and **11** (see Figure 7), as well as for bisligated $[NH_3{-}Ca{-}C_2H_2O_2]^{2+}$ and other Ca–N-bonded isomers (see the Supporting Information), are consistent with the fact that the monocations NH_4^+ (*m/z* 18), NH_3CH^+ (*m/z* 30), $NH_3CH_2^+$ (*m/z* 31), CaH^+ (*m/z* 41), NH_2Ca^+ (*m/z* 56), $CH_2CO_2H^+$ (*m/z* 59), $NH_2CHCO_2H^+$ (*m/z* 74), CO_2Ca^+ (*m/z* 84), CO_2HCa^+ (*m/z* 85), CCO_2HCa^+(*m/z* 97), and $CHCO_2Ca^+$ (*m/z* 97), or the dications NH_3Ca^{2+} (*m/z* 28.5) and $CaCO_2CH_2^{2+}$ (*m/z* 49), are not observed experimentally. The computations also provide a rationalization as to why *m/z* 32, 57, 60 and 85 are the only significant peaks in the MS/MS spectra. The Coulomb explosion reaction pathways that yield these product ions have barriers that are lower than those we have found for pathways leading to any of the other fragmentation products (see Figure 6 and 7 and the Supporting Information). In addition, these combinations of product ions are by

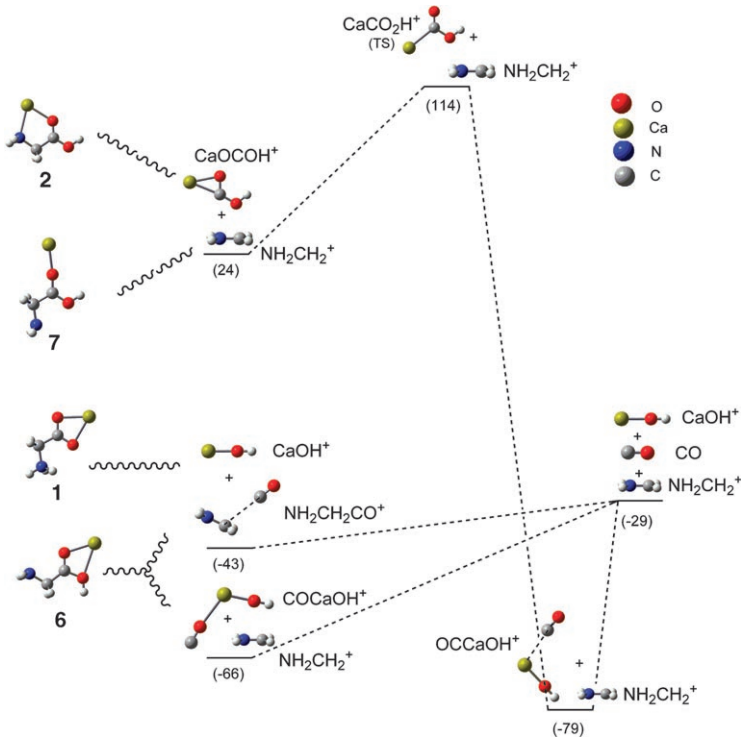

Figure 8. Simplified scheme showing the most important Coulomb explosion processes (waved lines) for isomers **1** and **2** of $[Ca(gly)]^{2+}$, either directly or via the intermediates **6** or **7**. Also shown are the energy profiles corresponding to the unimolecular decompositions (dashed lines) of the initially formed $[Ca,C,O_2,H]^+$ and $NH_2CH_2CO^+$ species. These provide an explanation for the greater relative intensities of the peaks in the MS/MS spectrum in Figure 2b at *m/z* 32 and 57 compared with 85 and 60. Relative energies ($kJ\,mol^{-1}$) are given in parentheses.

far the most stable from a thermodynamic point of view (see Figure 6 and 7 and the Supporting Information).

Despite the inherent characteristics of Coulomb explosions, where the partner ions should yield equally intense peaks, the *m/z* 32 ($NH_2CD_2^+$) and *m/z* 57 ($CaOH^+$) peaks in Figure 2b are significantly more intense than their counterpart peaks at *m/z* 85 ($[Ca,C,O_2,H]^+$ and *m/z* 60 ($NH_2CD_2CO^+$), respectively. Although part of the available energy in a Coulomb explosion process will appear as kinetic energy of the fragments,[18] these fragment ions are likely to retain sufficient internal energy from the CID to undergo spontaneous unimolecular decompositions. The intensity differences mentioned above may then be attributed to the $NH_2CD_2CO^+$ and $[Ca,C,O_2,H]^+$ species decomposing by loss of CO (in either single- or two-step processes) into $NH_2CD_2^+$ (*m/z* 32) and $CaOH^+$ (*m/z* 57), respectively (Scheme 1 and Figure 8). This leads not only to a decrease in the intensity of the *m/z* 85 and *m/z* 60 spectral lines, but in a concomitant increase in the intensity of the peaks at *m/z* 32 and *m/z* 57. This results in (neutral) carbon monoxide being produced, but it is of course a secondary product arising from the unimolecular decomposition of primary monocation products formed in the Coulomb explosions rather than being associated with dication fragmentations.

Comparison between the reactions of $[Ca(urea)]^{2+}$ and $[Ca(gly)]^{2+}$: The reactions of Ca^{2+} with urea and glycine show substantial differences. For $[Ca(urea)]^{2+}$, unimolecular processes that lead to loss of neutral fragments (e.g., NH_3, HNCO) compete with the Coulomb explosions that lead to monocations (e.g., $CaNH_2^+ + NH_2CO^+$ and $CaOCN^+ + NH_4^+$). In contrast, the $[Ca(gly)]^{2+}$ reaction products originate virtually exclusively from Coulomb explosion processes, the only notable exception corresponding to loss of NH_3 for which the observed peak is too weak for this reaction path to be considered competitive. In other words, while in the $[Ca(urea)]^{2+}$ reactions we have both monocations and dications as products, only monocations are formed in significant quantities for the $[Ca(gly)]^{2+}$ reactions. These differences can be understood by looking at the characteristics of the corresponding PESs. In the reactions of $[Ca(urea)]^{2+}$, some of the Coulomb explosions, for example those leading to NH_4^+ products, must be preceded by several hydrogen-transfer processes that involve reaction barriers similar to or higher than those associated with the H-shifts required for neutral (e.g., NH_3) loss.[20] Consequently, because of spontaneous NH_3 loss, the population of precursors able to yield NH_4^+ is small. In contrast, the $[Ca(gly)]^{2+}$ Coulomb explosions have barriers much lower than the alternative pathways.

Conclusion

Reactions between Ca^{2+} and glycine have been studied under electrospray mass spectrometry conditions. A theoretical characterization of the $[Ca(gly)]^{2+}$ potential energy surface shows that the global minimum corresponds to Ca^{2+} coordinated to the two oxygen atoms of zwitterionic glycine in a bridged structure, **1**. Since the zwitterionic form of glycine is dominant in solution, and taking into account the mild conditions associated with electrospray techniques, complex **1** should also be dominant in the mass spectrometer. The computed binding energy between neutral glycine and Ca^{2+} ($516\,kJ\,mol^{-1}$) is larger than that calculated for urea ($453\,kJ\,mol^{-1}$) at the same level of theory. The large binding energy between glycine and Ca^{2+} explains why all the mech-

anisms leading to the experimentally observed products involve stationary points on the PES that lie well below the entrance channel. The calculated PES indicates that the most favorable reaction processes correspond to Coulomb explosions originating mainly (and perhaps exclusively) from the zwitterionic complex **1** but perhaps also from the complex of Ca^{2+} with neutral glycine, **2**, either through direct reactions or via intermediates **6** and **7**. These Coulomb explosions lead to final products that lie 43 and 66 kJ mol^{-1} below **1**. These products in turn can account for the four intense peaks ($[Ca,C,O_2,H]^+$, $NH_2CH_2^+$, $CaOH^+$ and $NH_2CH_2CO^+$) observed in the MS/MS spectra. Bisligated $[NH_3{-}Ca{-}C_2H_2O_2]^{2+}$ complexes do not play a significant role in the reactivity of the system. Carbon monoxide is a secondary product of the $[Ca(gly)]^{2+}$ reactions, produced by the unimolecular decomposition of some of the primary ions formed in the Coulomb explosions.

In contrast to findings for the reactions of $[Ca(urea)]^{2+}$, in which some of the fragmentation products are molecular dications arising from the loss of a neutral fragment, no dications are found among the products in the $[Ca(gly)]^{2+}$ reactions. The difference in behavior between $[Ca(urea)]^{2+}$ and $[Ca(gly)]^{2+}$ can be readily explained in terms of the topological differences between their respective PESs.

Acknowledgements

This work has been partially supported by the DGI Project No. BQU2003–00894, by the COST Action D26/0014/03. I.C. gratefully acknowledges an FPU grant from the Ministerio de Educación y Ciencia of Spain. O.M. thanks the Ministerio of Educación, Cultura y Deporte of Spain for a Visiting Fellowship to the University of Sydney. D.M. thanks the University of Sydney for a Sesqui Postdoctoral Fellowship. L.R. thanks the Australian Research Council for a Discovery Grant and funding for the ARC Centre of Excellence in Free Radical Chemistry and Biotechnology, and gratefully acknowledges generous allocations of computer time from the ANU Supercomputing Facility (ANUSF), the Australian Partnership for Advanced Computing (APAC), and the Australian Centre for Advanced Computing and Communications (AC3).

[1] M. A. Kurinovich, J. K. Lee, *J. Am. Chem. Soc.* **2000**, *122*, 6258–6262.
[2] A. C. Drohat, J. T. Stivers, *J. Am. Chem. Soc.* **2000**, *122*, 1840–1841.
[3] M. A. Kurinovich, J. K. Lee, *J. Am. Soc. Mass Spectrom.* **2002**, *13*, 985–995.
[4] R. M. Moision, P. B. Armentrout, *Phys. Chem. Chem. Phys.* **2004**, *6*, 2588–2599.
[5] A. Luna, B. Amekraz, J. P. Morizur, J. Tortajada, O. Mó, M. Yáñez, *J. Phys. Chem. A* **2000**, *104*, 3132–3141.
[6] C. H. S. Wong, F. M. Siu, N. L. Ma, C. W. Tsang, *J. Mol. Struct.* **2002**, *588*, 9–16.
[7] M. Alcamí, O. Mó, M. Yáñez, A. Luna, J. P. Morizur, J. Tortajada, *J. Phys. Chem. A* **1998**, *102*, 10120–10127.
[8] B. A. Cerda, C. Wesdemiotis, *J. Am. Chem. Soc.* **1996**, *118*, 11884–11892.
[9] L. Rodríguez-Santiago, M. Sodupe, J. Tortajada, *J. Phys. Chem. A* **2001**, *105*, 5340–5347.
[10] Y. Hoppilliard, G. Ohanessian, S. Bourcier, *J. Phys. Chem. A* **2004**, *108*, 9687–9696.
[11] J. J. R. Fraudo da Silva, R. J. P. Williams, *The Biological Chemistry of Elements*, Oxford University Press, Oxford, **1991**.
[12] S. Forsen, J. Kordel, *Bioinorganic Chemistry*, University Science Books, Mill Valley, California, **1994**.
[13] T. Masuoka, *J. Chem. Phys.* **1993**, *98*, 6989–6994.
[14] D. Mathur, *Phys. Rep.* **1993**, *225*, 193–272.
[15] C. S. O'Connor, S. D. Price, *Int. J. Mass Spectrom.* **1999**, *184*, 11–23.
[16] P. Jayaweera, A. T. Blades, M. G. Ikonomou, P. Kebarle, *J. Am. Chem. Soc.* **1990**, *112*, 2452–2454.
[17] D. Schröder, H. Schwarz, *J. Phys. Chem. A* **1999**, *103*, 7385–7394.
[18] a) D. Schröder, *Angew. Chem.* **2004**, *116*, 1351–1353; *Angew. Chem. Int. Ed.* **2004**, *43*, 1329–1331.
[19] I. Corral, O. Mó, M. Yáñez, J.-Y. Salpin, J. Tortajada, L. Radom, *J. Phys. Chem. A* **2004**, *108*, 10080–10088.
[20] I. Corral, O. Mó, M. Yáñez, A. Scott, L. Radom, *J. Phys. Chem. A* **2003**, *107*, 10456–10461.
[21] A. D. Becke, *J. Chem. Phys.* **1993**, *98*, 1372–1377.
[22] C. Lee, R. G. Parr, *Phys. Rev. A* **1990**, *42*, 193–200.
[23] M. J. Frisch, G. W. Trucks, H. B. Schlegel, G. E. Scuseria, M. A. Robb, J. R. Cheeseman, V. G. Zakrzewski, J. J. A. Montgomery, T. Vreven, K. N. Kudin, J. C. Burant, J. M. Millam, S. S. Iyengar, J. Tomasi, V. Barone, B. Mennucci, M. Cossi, G. Scalmi, N. Rega, G. A. Petersson, H. Nakatsuji, M. Hada, M. Ehara, K. Toyota, R. Fukuda, J. Hasegawa, M. Ishida, T. Nakajima, Y. Honda, O. Kitao, C. Adamo, J. Jaramillo, R. Gomperts, R. E. Stratmann, O. Yazyev, J. Austin, R. Cammi, C. Pomelli, J. Ochterski, P. Y. Ayala, K. Morokuma, G. A. Voth, P. Salvador, J. J. Dannenberg, V. G. Zakrzewski, S. Dapprich, A. D. Daniels, M. C. Strain, O. Farkas, D. K. Malick, A. D. Rabuck, K. Raghavachari, J. B. Foresman, J. V. Ortiz, Q. Cui, A. G. Baboul, S. Clifford, J. Cioslowski, B. B. Stefanov, G. Liu, A. Liashenko, P. Piskorz, I. Komaromi, R. L. Martin, D. J. Fox, T. Keith, M. A. Al-Laham, C. Y. Peng, A. Nanayakkara, M. Challacombe, P. M. W. Gill, B. Johnson, W. Chen, M. W. Wong, C. Gonzalez, J. A. Pople, Gaussian 03, Revision C.02, Gaussian Inc., Wallingford CT, **2003**.
[24] M. A. Iron, M. Oren, J. M. L. Martin, *Mol. Phys.* **2003**, *101*, 1345–1361.
[25] A. Schulz, B. J. Smith, L. Radom, *J. Phys. Chem. A* **1999**, *103*, 7522–7527.
[26] M. B. Sullivan, M. A. Iron, P. C. Redfern, J. M. L. Martin, L. A. Curtiss, L. Radom, *J. Phys. Chem. A* **2003**, *107*, 5617–5630.
[27] R. F. W. Bader, *Atoms in Molecules. A Quantum Theory*, Clarendon Press, Oxford, **1990**.
[28] M. Beyer, E. R. Williams, V. E. Bondybey, *J. Am. Chem. Soc.* **1999**, *121*, 1565–1573.
[29] S. Hoyau, J.-P. Pélicier, F. Rogalewicz, Y. Hoppilliard, G. Ohanessian, *Eur. J. Mass Spectrom.* **2001**, *7*, 303–311.
[30] E. F. Strittmatter, A. S. Lemoff, E. R. Williams, *J. Phys. Chem. A* **2000**, *104*, 9793–9796.
[31] S. Hoyau, G. Ohanessian, *J. Am. Chem. Soc.* **1997**, *119*, 2016–2024.
[32] S. Hoyau, G. Ohanessian, *Chem. Eur. J.* **1998**, *4*, 1561–1569.
[33] J. Bertrán, L. Rodríguez-Santiago, M. Sodupe, *J. Phys. Chem. B* **1999**, *103*, 2310–2317.
[34] Note that for simplicity, the molecular formulae of the fragments in the ensuing discussion are written in terms of the non-isotopically-labeled species. However, the mass-to-charge ratio (m/z) specified within the text may correspond (when indicated) to the MS/MS involving the 2,2-[D_2]-glycine isotopomer, as displayed in Figure 2b, in order to allow a better comparison with the experimental results.

Received: January 30, 2006
Revised: May 15, 2006
Published online: June 28, 2006

